Experimental study of a novel subcooling method based on liquid desiccant dehumidification for vapor-compression refrigeration systems

She, Xiaohui; Yin, Yonggao; Luo, Yimo; Lindeman, Brett; Zhong, Dan; Zhang, Xiaosong

DOI:
10.1016/j.applthermaleng.2017.11.011

Document Version
Peer reviewed version

Citation for published version (Harvard):
She, X, Yin, Y, Luo, Y, Lindeman, B, Zhong, D & Zhang, X 2018, 'Experimental study of a novel subcooling method based on liquid desiccant dehumidification for vapor-compression refrigeration systems', Applied Thermal Engineering, vol. 130, pp. 1460-1471. https://doi.org/10.1016/j.applthermaleng.2017.11.011

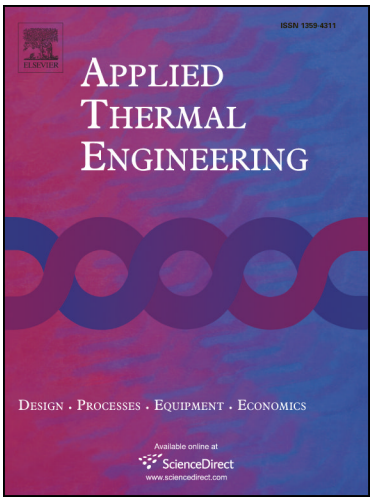

Experimental study of a novel subcooling method based on liquid desiccant dehumidification for vapor-compression refrigeration systems

Xiaohui She, Yonggao Yin, Yimo Luo, Brett Lindeman, Dan Zhong, Xiaosong Zhang

PII: S1359-4311(17)32714-X
DOI: https://doi.org/10.1016/j.applthermaleng.2017.11.011
Reference: ATE 11381

To appear in: *Applied Thermal Engineering*

Received Date: 21 April 2017
Revised Date: 17 September 2017
Accepted Date: 3 November 2017

Please cite this article as: X. She, Y. Yin, Y. Luo, B. Lindeman, D. Zhong, X. Zhang, Experimental study of a novel subcooling method based on liquid desiccant dehumidification for vapor-compression refrigeration systems, *Applied Thermal Engineering* (2017), doi: https://doi.org/10.1016/j.applthermaleng.2017.11.011

Experimental study of a novel subcooling method based on liquid desiccant dehumidification for vapor-compression refrigeration systems

Xiaohui She[a,b], Yonggao Yin[b], Yimo Luo[c], Brett Lindeman[d], Dan Zhong[c], Xiaosong Zhang[b,*]

[a]*School of Chemical Engineering, University of Birmingham, Birmingham B15 2TT, UK*
[b]*School of Energy and Environment, Southeast University, Nanjing 210096, China*
[c]*Faculty of Science and Technology, Technological and Higher Education Institute of Hong Kong, Hong Kong, China*
[d] *Department of Mechanical Engineering, University of Wisconsin-Madison, Madison, 53706, USA*

***Corresponding author:** Xiaosong Zhang, PhD.
Email: rachpe@seu.edu.cn

Abstract

Refrigerant subcooling could increase the refrigerating capacity and potentially improve the performance of refrigeration systems. In this paper, a novel subcooling method is experimentally studied for the first time in a hybrid vapor compression refrigeration system. In this system, condensation heat (around 40 ^{o}C) is used to drive an integrated subcooling cycle to subcool the refrigerant leaving the condenser, which significantly increases the system performance. Changes in system performance are measured as functions of the following variables: the mass flow rates of the dehumidification air, ambient air, dehumidification solution, regeneration solution, and spraying water. Comparisons are made between the proposed system and the traditional water-cooled chiller. The proposed system can achieve a larger degree of subcooling (15-20 ^{o}C); what's more, it shows much higher performances than the traditional water-cooled chiller: *COP* of the chiller is improved by 18.6%, and the exergy efficiency is increased up to 27.9%. Performance of the integrated subcooling cycle is also evaluated; it has a low *COP*, with the maximum value of 0.13, due to the low-grade condensation heat; however, it has a pretty high exergy efficiency, with the maximum value of 0.28, which indicates

the effective use of the low-grade heat. In addition, an economic analysis of the integrated subcooling cycle is made with a project life cycle of 15 years; the payback period varies from 2.4 to 3.2 years based on different electricity tariffs, and the savings to investment ratio is between 1.3 and 2.1, which indicates that the project is profitable.

Keywords: subcooling; liquid desiccant; evaporative cooling; exergy analysis; economic analysis.

Nomenclatures

AS	annual savings ($)
a_w	specific surface area of the packing (m^2/m^3)
COP	coefficient of performance
Cp	specific heat capacity(kJ/kg ^oC)
D	depth (m)
e	specific exergy (kJ/kg)
E	error (%)
G	air mass flow rate (kg/s)
h	specific enthalpy (kJ/kg)
H	height (m)
L	length (m)
M	liquid mass flow rate (kg/s)
N	number of years
NPV	net present value ($)
PV_I	present value of investment ($)
PV_S	present value of savings ($)

Q	heat capacity (kW)
r_d	discount rate
r_{in}	inflation rate
s	specific entropy (kJ/kg K)
SIR	savings to investment ratio
SPP	simple payback period (year)
T	temperature (^oC)
W	power consumption (kW)
X	concentration (%)

Greek symbols

Δ	difference
ω	humidity ratio (kg/kg)

Subscripts

a	air
amb	ambient air
base	traditional water-cooled chiller
ch	chiller cycle
com	compressor
con	condenser
deh	dehumidifier
eva	evaporator
EC	evaporative cooler

imp	improvement
in	input
lat	latent
out	output
r	regeneration
ref	refrigerant
reg	regenerator
s	solution
sen	sensible
sub	integrated subcooling
w	water

1. Introduction

With the rapidly improving economy and increasing urbanization, energy consumption in buildings has increased significantly and accounts for 27% of the national energy consumption in China; energy consumption from air conditioning is about 53% of that consumed energy [1]. Therefore, it is urgent to reduce the energy consumption of air conditioning systems.

Refrigerant subcooling can increase the refrigerating capacity and potentially improve the coefficient of performance (*COP*) of air conditioning systems. From the perspective of the second law of thermodynamics, refrigerant subcooling reduces throttling losses resulting from an isenthalpic expansion [2]. The traditional method usually adds a liquid-suction heat exchanger between the outlets of the condenser and evaporator [3-7]. Kleinet al. [3] analyzed how pressure drops through the liquid-suction heat exchanger affected the system performance with different refrigerants. Hermes [5]

reported a study of the potential for refrigerant charge reduction in vapor compression refrigeration systems by means of a liquid-suction heat exchanger. Experimental analysis of how a liquid-suction heat exchanger can affect the performance of a vapor compression refrigeration system was made using R1234yf [6], R1234ze(E) and R450A [7]. The liquid-suction heat exchanger achieves subcooling by transferring the refrigerant heat from the condenser outlet to the compressor inlet. The larger degree of superheat at the compressor inlet results in decreased refrigerant flow, thereby reducing the system performance. In order to eliminate the drawbacks of the liquid-suction heat exchanger, some researchers use a mechanical subcooling method, in a refrigeration system, to enhance the system *COP* and also to decrease the degree of superheat [8-12]. In the mechanical subcooling method, a small mechanical vapor compression cycle is coupled to the main refrigeration cycle, at the exit of the condenser, to provide subcooling to the main refrigeration cycle. Yang and Zhang [8] presented a model-based comprehensive analysis on such a subcooler design and discussed the optimal subcooling control. Qureshi and Zubair [9] analyzed the impact of fouling on performance of the vapor compression refrigeration system with integrated mechanical subcooling. Qureshiet al. [11] experimentally investigated how the use of a dedicated mechanical subcooling cycle affected the system performance. The experimental results indicated that the refrigerating capacity increased by approximately 0.5 kW, and the second-law efficiency of the cycle increased by an average of 21%. Because the mechanical subcooling method needs an additional compressor to provide the driving force of subcooling, the electricity consumption of the compressor will carry an undesirable effect on the system *COP*. Considering that, some researchers utilize phase change materials (PCM) and heat pipes, in cold storage units, as a subcooler [13-16]. Hsiao et al. [14] investigated the thermal performance of a heat pump system, with an ice storage subcooler, to supply heating and cooling

demands to two greenhouses, respectively. The results showed that in the charge mode, the heat pump *COP* of the ice storage system was 12% higher than that without the ice storage system; in the discharge mode, the ice storage system provided the refrigerator a *COP* 15% higher than that without the ice storage system. Huang et al. [15] experimentally investigated the performance of a cold storage air conditioning system that utilized a thermal battery as a subcooler, which gave 28% more refrigerating capacity and 8% higher *COP*.

A novel subcooling method, based on liquid desiccant dehumidification, was proposed and analyzed in our previous work [17-20]. In this method, condensation heat from the condenser is used to drive liquid desiccant dehumidification for dry air, which is later to absorb moisture from spray water and low temperature cooling water is then obtained to subcool the refrigerant leaving the condenser. Thermodynamic analyses and optimizations of the proposed system have shown good performance improvement. However, these are only from theoretical perspectives, no experimental work is found in the literature. In this paper, an experimental setup is built and tested to complement the previous theoretical studies, and further provide proof of the proposed subcooling method in reality. Changes in system performance are measured as functions of mass flow rates for the following entities: the dehumidification air (G_a), the ambient air (G_{amb}), the dehumidification solution ($m_{s,deh}$), the regeneration solution ($m_{s,reg}$), and the spraying water ($m_{w,EC}$). Both the first law and second law thermodynamic analyses are conducted on the proposed system, and comparisons are made between the proposed system and the traditional water-cooled chiller. In addition, economic benefits of the proposed system are also evaluated with a life cycle of 15 years.

2. Experimental setup and procedure

2.1. System description

The hybrid vapor-compression refrigeration system, realizing the proposed subcooling method, consists of a chiller cycle and an integrated subcooling cycle, as shown in Fig. 1. The integrated subcooling cycle is similar to the double-stage absorption refrigeration cycle driven by low-grade heat, and can be divided into an evaporative cooling cycle and a liquid desiccant dehumidification cycle. The liquid desiccant dehumidification cycle driven by condensation heat (around 40 ^{o}C) is used to produce dry air for the evaporative cooling cycle, where low-temperature cooling water is obtained to subcool the refrigerant leaving the condenser and correspondingly the increase of the refrigerating capacity is expected.

Fig. 2 is the picture of the experimental setup of the proposed system. In the chiller cycle, the refrigerant temperature is measured using a Pt100 platinum resistor, and pressure is measured by the pressure transmitter. Power consumption of the compressor is measured by a WT230 power meter. The chilled water temperature is measured using a type-T thermocouple, and the mass flow rate is measured using a turbine flowmeter. In the evaporative cooling cycle, the temperature and humidity, of the air leaving the evaporative cooler and dehumidifier, are measured by a Rotronic temperature and humidity transmitter. The air temperature entering the evaporative cooler and dehumidifier is measured by a type-T thermocouple. The mass flow rate of the air is measured by the KIMO flow meter. In the liquid desiccant dehumidification cycle, the solution temperature is measured using type-T thermocouples, and the mass flow rate is measured using an electromagnetic flow meter. The temperature and humidity of the ambient air at the inlet and outlet of the regenerator are measured using the Rotronic temperature and humidity transmitter, while the mass flow rate is measured by the KIMO flow meter. The cooling water temperature, at the inlet and outlet of the solution cooler, is measured using a type-T thermocouple. Parameters of the measuring instruments are shown in Table 1.

R22 is used in the chiller cycle which is due to the fact that, for such a small chiller, R22 is commonly used for the compressor in the market of China. The properties of R22 are obtained from REFPROP 8.0. LiCl solution is chosen for the liquid desiccant dehumidification cycle, and its properties could be found in the literature [21]. Fig. 3 shows the P-h diagram of refrigerants and T-d diagram of air and solution.

2.2. The first law thermodynamic performance index

The humidity ratio difference of air ($\Delta\omega_a$), between the inlet and outlet of the dehumidifier, and moisture removal rate in the dehumidifier (m_{deh}) are calculated using the following equations,

$$\Delta\omega_a = \omega_8 - \omega_9 \tag{1}$$

$$m_{deh} = G_a \cdot \Delta\omega \tag{2}$$

where, G_a is the mass flow rate of the air in the dehumidifier. The humidity ratios, ω_8 and ω_9, are located at the inlet and outlet of the dehumidifier, respectively.

The difference in humidity ratio for the ambient air ($\Delta\omega_{amb}$), between the outlet and inlet of the regenerator, and moisture removal rate in the regenerator (m_r) are obtained by Eqs. (3) and (4), respectively,

$$\Delta\omega_{amb} = \omega_{20} - \omega_{19} \tag{3}$$

$$m_r = G_{amb} \cdot \Delta\omega \tag{4}$$

where, G_{amb} is the mass flow rate of ambient air in the regenerator, and humidity ratios of the ambient air, ω_{19} and ω_{20}, are located at the inlet and outlet of the regenerator, respectively.

In the evaporative cooler, the dry air absorbs moisture (m_{EC}) from the spraying water via latent heat transfer ($Q_{EC,lat}$), one part of which is to cool the air ($Q_{EC,sen}$), and the other part is to subcool the refrigerant (Q_{sub}).

$$m_{EC} = G_a \cdot (\omega_7 - \omega_{10}) \quad (5)$$

$$Q_{EC,lat} = m_{EC} \cdot 2500 \quad (6)$$

$$Q_{EC,sen} = Cp_a \cdot G_a \cdot (T_{10} - T_7) \quad (7)$$

where, humidity ratios of the air, ω_{10} and ω_7, are located at the inlet and outlet of the evaporative cooler, respectively. The specific heat capacity of the air is denoted by Cp_a, while air temperatures T_{10} and T_7 are located at the inlet and outlet of the evaporative cooler, respectively.

The degree of subcooling (ΔT_{sub}), performance of the chiller cycle (COP_{ch}), and performance of the integrated subcooling cycle (COP_{sub}), are calculated as follows,

$$\Delta T_{sub} = T_{con} - T \quad (8)$$

$$COP_{ch} = \frac{Cp_w \cdot m_{w,eva} \cdot (T_{22} - T_{21})}{W_{com}} \quad (9)$$

$$COP_{sub} = \frac{Cp_w \cdot m_{w,EC} \cdot (T_6 - T_5)}{Cp_s \cdot m_{s,reg} \cdot (T_{14} - T_{13})} \quad (10)$$

where, T_4 is the refrigerant temperature at the outlet of the subcooler; the mass flow rate of chilled water is $m_{w,eva}$; $m_{s,reg}$ is the mass flow rate of the solution in the condenser; $m_{w,EC}$ is the mass flow rate of the low temperature cooling water in the subcooler; and the power consumption of the compressor is W_{com}.

Comparisons are made between the proposed system and the traditional water-cooled chiller. To allow for comparison, several assumptions are made on the water-cooled chiller: (1) condensing temperature is 11 ^{o}C higher than the cooling water temperature at the outlet of cooling tower [22]; (2) the evaporating temperature and compressor efficiency are the same as that of the proposed system; (3) both the degree of refrigerant superheat and degree of subcooling are 5 ^{o}C.

Chiller performance improvement (COP_{imp}) is defined in the following manner,

$$COP_{imp} = \frac{COP_{ch} - COP_{base}}{COP_{base}} \tag{11}$$

where, COP_{base} is the performance of the traditional water-cooled chiller.

2.3. The second law thermodynamic performance index

Besides the *COP*, exergy efficiency is also an important performance index which indicates the irreversible energy loss during heat transfer. In the chiller cycle, the input exergy includes the power consumption of the compressor and the exergy of the spaying water in the subcooler; the output exergy consists of the exergy of the chilled water in the evaporator and the exergy of the solution in the condenser. Therefore, the exergy efficiency of the chiller cycle is defined as,

$$\eta_{ch} = \frac{m_{w,eva} \cdot (e_{21} - e_{22}) + m_{s,reg} \cdot (e_{14} - e_{13})}{m_{w,EC} \cdot (e_5 - e_6) + W_{com}} \tag{12}$$

where, e_{13} and e_{14} are the exergy of the solution at the inlet and outlet of the condenser, respectively; e_5 and e_6 are the exergy of the spray water at the inlet and outlet of the subcooler, respectively; e_{21} and e_{22} are the exergy of the chilled water at the outlet and inlet of the evaporator, respectively; both the exergy of water and solution can be calculated in the following equation:

$$e = Cp \cdot ((T - T_{amb}) - T_{amb} \cdot \ln \frac{T}{T_{amb}}) \tag{13}$$

Exergy efficiency improvement (η_{imp}) of the chiller is defined as,

$$\eta_{imp} = \frac{\eta_{ch} - \eta_{ba}}{\eta_{base}} \tag{14}$$

where, η_{base} is the exergy efficiency of the traditional water-cooled chiller.

For the integrated subcooling cycle, the exergy input is the exergy of the condensing heat in the condenser and the exergy output is the exergy of the increased refrigerating capacity in the evaporator. Hence, the exergy efficiency of the integrated subcooling cycle is defined as,

$$\eta_{sub} = \frac{e_{4'} - e_{3'}}{e_2 - e_3} \tag{15}$$

where, e_2-e_3 is the specific exergy input of the refrigerant in the condenser, and $e_{4'}$ -$e_{3'}$ is the specific

exergy output of the refrigerant in the evaporator; the specific exergy of the refrigerant is calculated by,

$$e_{ref} = h - h_{amb} - T_{amb} \cdot (s - s_{amb}) \tag{16}$$

where, T_{amb} and h_{amb} are the temperature and specific enthalpy of the refrigerant at ambient conditions, respectively.

2.4. Economic performance index

In order to evaluate the economic benefit of the use of the integrated subcooling cycle, an economic analysis with life cycle costs is carried out using the annualized cash flows [23].

The present value of investments (PV_I) is:

$$PV_I = \sum_{t=0}^{N-1} I_t \cdot \left(\frac{1+r_{in}}{1+r_d}\right)^t - \frac{\text{Res. Val.}}{(1+r_d)^N} \tag{17}$$

The present value of savings (PV_S) is:

$$PV_S = \sum_{t=1}^{N} AS_t \cdot \frac{1}{(1+r_d)^t} \tag{18}$$

where, N is the number of years of the project life-span; r_d is the discount rate; r_{in} is the inflation rate; AS is the annual savings; Res. Val. is the residual value of the component.

The net present value (NPV) is the life cycle net savings of a project and is calculated by,

$$NPV = PV_S - PV_I \tag{19}$$

The savings to investment ratio (SIR) is another parameter which indicates the profitability of a project, and is defined as,

$$SIR = \frac{PV_S}{PV_I} \tag{20}$$

Simple payback period (SPP), expressed in years, refers to the length of time that it takes for a project to recoup its initial investment.

$$SPP = \frac{\text{Capital cost}}{\text{Savings/year}} \tag{21}$$

2.5. Energy balance

Before analyzing the experimental data, it is necessary to study the energy balance of the proposed system. Here, the chiller cycle is studied; the refrigerant pipes, evaporator, condenser, and subcooler are covered by thermal insulation materials. In the chiller cycle, the input energy (Q_{in}) includes refrigerating capacity (Q_{eva}) and power consumption of the compressor (W_{com}). The output energy (Q_{out}) consists of the condensation heat capacity (Q_{con}) and subcooling capacity (Q_{sub}).

$$Q_{in} = Q_{eva} + W_{com} \tag{22}$$

$$Q_{out} = Q_{con} + Q_{sub} \tag{23}$$

The energy balance error (E) is defined as follows:

$$E = \frac{abs(Q_{in} - Q_{out})}{\max(Q_{in}, Q_{out})} \tag{24}$$

Table 2 shows the energy balance of the experimental chiller cycle with different working conditions. As shown, the energy balance error (E) is within 10% of theory; therefore, the experimental data is reliable for the following analysis.

3. Experimental results and discussion

In the hybrid vapor compression refrigeration system, several working parameters affect the system performance. The key parameters include the mass flow rate of the dehumidification air (G_a), the mass flow rate of ambient air (G_{amb}), the mass flow rate of dehumidification solution ($m_{s,deh}$), the mass flow rate of regeneration solution ($m_{s,reg}$), and the mass flow rate of the spraying water ($m_{w,EC}$). During the experiment, there are no devices to control the temperature and humidity of the ambient air (T_{amb} and ω_{amb}). As a result, such ambient air parameters are slightly variable. Working parameters, including the solution concentration (X_s) and chilled water mass flow rate ($m_{w,eva}$), are shown in Table 3, where the solution mass flow rate in the solution heat exchanger is 0.28 kg/s.

3.1 Effects of varying the mass flow rate of the dehumidification air

Fig. 4(a) shows how varying the mass flow rate of the dehumidification air (G_a) affects the difference in the humidity ratio between the inlet and outlet of the dehumidifier ($\Delta\omega_a$) and the moisture removal rate in the dehumidifier (m_{deh}). When G_a increases from 0.14 kg/s to 0.33 kg/s, $\Delta\omega_a$ decreases significantly from 2 g/kg to 1.7 g/kg. This is because the increase of G_a makes the air flow faster for a given dehumidifier packing size. This leads to shorter contact time between the air and the solution, resulting in lower dehumidification of the air per unit mass. In addition, with the increase of G_a, m_{deh} increases significantly from 0.27 g/s to 0.57 g/s. Despite the decreased $\Delta\omega_a$, the increase of G_a results in the increase of m_{deh}.

Fig. 4(b) shows how varying the mass flow rate of dehumidification air (G_a) affects the performance of the evaporative cooler. When G_a increases from 0.14 kg/s to 0.33 kg/s, the sensible heating of air ($Q_{EC,sen}$) increases significantly from 0.26 kW to 0.94 kW, and latent heating ($Q_{EC,lat}$) rises dramatically from 0.68 kW to 1.43 kW. The increase of sensible heating is due to more air needing to be cooled with the increased G_a, and the increase of latent heating results from the increase of moisture removal rate in the evaporative cooler. In addition, with the increase of G_a, the subcooling (Q_{sub}) increases gradually from 0.43 kW to 0.56 kW, and then decreases generally to 0.48 kW, which comes from the combined effects of latent and sensible heating.

Fig. 5 shows how varying the mass flow rate of dehumidification air (G_a) affects system performance. As shown in Fig. 5(a), with the increase of G_a, the condensing temperature (T_{con}) decreases gradually and then increases, which is mainly due to changes in the condenser's solution temperature. With the increase of G_a, the moisture removal rate in the dehumidifier increases. Correspondingly, the solution temperature at the outlet of the dehumidifier increases, and the solution concentration becomes weaker. This improves the regeneration effect in the regenerator, and decreases

the solution temperature at the outlet of the regenerator. Due to the changes of solution temperature at the outlet of the regenerator and dehumidifier, the temperature of the mixed solution at the inlet of the condenser decreases initially and subsequently increases. In addition, the degree of subcooling (ΔT_{sub}) shows the same trends as the condensing temperature.

Fig. 5(b) shows how varying the mass flow rate of dehumidification air (G_a) affects the refrigerating capacity (Q_{eva}) and power consumption of the compressor (W_{com}). When G_a increases from 0.14 kg/s to 0.27 kg/s, Q_{eva} increases gradually from 4.38 kW to 4.59 kW; while G_a increases from 0.27 kg/s to 0.33 kg/s, Q_{eva} decreases gradually to 4.42 kW. In addition, with the increase of G_a, W_{com} initially decreases and then increases, which is mainly affected by the condensing temperature. When G_a is 0.2 kg/s, W_{com} has a minimum value 1.28 kW.

Varying the mass flow rate of the dehumidification air (G_a) affects the COP_{ch} and COP_{sub} as shown in Fig. 5(c). When G_a increases from 0.14 kg/s to 0.27 kg/s, COP_{ch} increases gradually from 3.29 to 3.54 and COP_{sub} increases generally from 0.08 to 0.12, which is mainly due to the decrease of condensing temperature; while G_a increases from 0.27 kg/s to 0.33 kg/s, COP_{ch} decreases gradually to 3.36 and COP_{sub} decreases to 0.1, which mainly results from the increase of condensing temperature. When G_a is around 0.25 kg/s, system performance achieves a maximum value. In addition, compared with the traditional water-cooled chiller, the proposed system has a higher COP_{ch}. As shown in Fig. 5(d), the maximum chiller performance improvement (COP_{imp}) is 9.2%.

3.2 Effects of varying the mass flow rate of the ambient air

Fig. 6 shows how varying the mass flow rate of ambient air (G_{amb}) affects the humidity ratio difference of the ambient air between the outlet and inlet of the regenerator ($\Delta\omega_{amb}$) and the moisture removal rate in the regenerator (m_r). With the increase of G_{amb}, $\Delta\omega_{amb}$ decreases significantly from 6.1

g/kg to 2.9 g/kg. This is because the ambient air and solution have less contact time when the packing size of the regenerator is held constant; correspondingly the humidification effect of ambient air per unit mass will decrease. When G_{amb} increases from 0.16 kg/s to 0.25 kg/s, m_r decreases significantly from 0.98 g/s to 0.76 g/s, due to the accompanying decrease of $\Delta\omega_{amb}$. As G_{amb} increases from 0.25 kg/s to 0.27 kg/s, m_r increases gradually to 0.8 g/s, because G_{amb} increases more than the associated decrease in $\Delta\omega_{amb}$.

Fig. 7 shows how varying the mass flow rate of ambient air (G_{amb}) affects the performance of the proposed system. As shown in Fig. 7(a), when G_{amb} increases from 0.16 kg/s to 0.21 kg/s, T_{con} decreases from 41.3 ^{o}C to 38.9 ^{o}C; while G_{amb} increases from 0.21 kg/s to 0.27 kg/s, T_{con} decreases from 38.9 ^{o}C to 38.1 ^{o}C. The decreased condensing temperature is due to the enhanced heat transfer between the ambient air and solution, which is a result of the increased G_{amb}. This leads to the decrease in solution temperature at the outlet of the regenerator, and further affects the condensing temperature. When G_{amb} is higher than 0.19 kg/s, condensing temperature of the proposed system is lower than that of the water-cooled chiller.

Fig. 7(b) shows how varying the mass flow rate of the ambient air (G_{amb}) affects the COP_{ch} and COP_{sub}. When G_{amb} increases from 0.16 kg/s to 0.21 kg/s, COP_{ch} increases from 3.67 to 4.16, which is due to the decrease of power consumption of compressor, while COP_{sub} decreases from 0.13 to 0.1, which mainly results from the decrease of subcooling capacity. When G_{amb} is higher than 0.21 kg/s, both COP_{ch} and COP_{sub} change slightly.

Fig. 7(c) shows the effect of varying the mass flow rate of the ambient air (G_{amb}) on the exergy efficiency of the chiller cycle (η_{ch}) and the integrated subcooling cycle (η_{sub}). With the increase of G_{amb}, η_{ch} increases slightly from 0.269 to 0.275 and then decreases to 0.269, which is a combined result of

the exergy decrease of the condensing heat and the power consumption decrease of the compressor; η_{sub} increases significantly from 0.19 to 0.23, which is mainly due to the exergy decrease of the condensing heat. It can be seen that the exergy efficiency of the integrated subcooling cycle is pretty high, only a little lower than that of the chiller cycle, which indicates the effective utilization of the condensing heat. In addition, the proposed system has a much better performance than the traditional water-cooled chiller. As shown in Fig. 7(d), the improvement of the exergy efficiency (η_{imp}) varies between 24% and 26.7%, and that of the coefficient of performance (COP_{imp}) could reach up to 18.6%.

3.3 Effects of varying the mass flow rate of the dehumidification solution

Fig. 8 shows the effect of varying the dehumidification solution mass flow rate ($m_{s,deh}$) on the humidity ratio difference of air between the inlet and outlet of the dehumidifier ($\Delta\omega_a$) and the moisture removal rate in the dehumidifier (m_{deh}).With the increase of $m_{s,deh}$, $\Delta\omega_a$ decreases slowly from 2.5 g/kg to 2.3 g/kg, and m_{deh} decreases slightly from 0.68 g/s to 0.61 g/s. This is because the increase of $m_{s,deh}$ (point 17) will increase the self-circulation of the dehumidifier solution (point 11r) when the solution mass flow rate in the solution heat exchanger (point 16) is held constant. This leads to the decreased solution concentration in the dehumidifier, and correspondingly decreases the dehumidification effect.

Fig. 9 shows the effect of varying the dehumidification solution mass flow rate ($m_{s,deh}$) on the condensing temperature (T_{con}), degree of subcooling (ΔT_{sub}), COP_{ch}, and COP_{sub} of the proposed system. As shown in Fig. 9(a), with the increase of $m_{s,deh}$, T_{con} increases slightly from 38.3 ^{o}C to 38.6 ^{o}C, and then decreases to 38.1 ^{o}C, which is the joint result of the decrease of solution temperature leaving the dehumidifier (point 11) and increase of solution temperature leaving the regenerator (point 15). ΔT_{sub} shows the same trends as T_{con}. Fig. 9(b) shows the effect of changing $m_{s,deh}$ on the COP_{ch} and COP_{sub}. With the increase of $m_{s,deh}$, the COP_{ch} increases gradually from 3.44 to 3.59, which is mainly

due to the increase of refrigerating capacity, while COP_{sub} decreases slightly at first, and then increases slightly, which mainly results from the changes of condensing temperature.

3.4 Effects of varying the mass flow rate of the regeneration solution

Fig. 10 shows how varying the mass flow rate of the regeneration solution ($m_{s,reg}$) affects the humidity ratio difference of the ambient air between the outlet and inlet of the regenerator ($\Delta\omega_{amb}$) and the moisture removal rate in the regenerator (m_r). When $m_{s,reg}$ increases from 0.4 kg/s to 0.52 kg/s, $\Delta\omega_{amb}$ increases from 4.26 g/kg to 4.32 g/kg. This is mainly due to the higher $m_{s,reg}$ being beneficial to the regeneration process. When $m_{s,reg}$ increases from 0.52 kg/s to 0.85 kg/s, $\Delta\omega_{amb}$ decreases from 4.32 g/kg to 3.92 g/kg. This is because, with the increase of $m_{s,reg}$, the solution mass flow rate of self-circulation in the regenerator (point 15r) will increases when the solution mass flow rate in the solution heat exchanger (point 12) is constant. Therefore, the mixed solution concentration entering the condenser (point 13) is stronger, which decreases the regeneration effect. In addition, m_r shows the same trends as $\Delta\omega_{amb}$.

Fig. 11 shows how varying the mass flow rate of regeneration solution ($m_{s,reg}$) affects the degree of subcooling (ΔT_{sub}), condensing temperature (T_{con}), COP_{ch} and COP_{sub} of the proposed system. As shown in Fig. 11(a), when $m_{s,reg}$ increases from 0.4 kg/s to 0.66 kg/s, T_{con} decreases from 39 ^{o}C to 38 ^{o}C; while $m_{s,reg}$ is higher than 0.66 kg/s, T_{con} remains almost constant. The gradual decrease of T_{con} is mainly due to the fact that as $m_{s,reg}$ increases, the solution temperature leaving the condenser decreases. The solution temperature at the outlet of the regenerator will be lower when the regeneration effect does not significantly vary. Therefore, the temperature of the mixed solution entering the condenser will decrease, which leads to the gradual decrease of T_{con}. In addition, ΔT_{sub} decreases slowly with the increase of $m_{s,reg}$. Fig. 11(b) shows how varying $m_{s,reg}$ affects the COP_{ch} and COP_{sub}. When $m_{s,reg}$

increases from 0.4 kg/s to 0.66 kg/s, COP_{ch} increases from 2.9 to 3.1 which is mainly due to the decrease of condensing temperature, while COP_{sub} decreases slightly from 0.11 to 0.1 which mainly results from the decrease of subcooling capacity; when $m_{s,reg}$ is higher than 0.66 kg/s, both COP_{ch} and COP_{sub} do not significantly vary.

3.5 Effect of varying the mass flow rate of the evaporative cooler's spraying water

Fig. 12 shows how varying the mass flow rate of spraying water in the evaporative cooler ($m_{w,EC}$) affects the performance of the evaporative cooler. As shown in Fig. 12(a), with the increase of $m_{w,EC}$, the relative humidity of the air at the outlet of the evaporative cooler increases from 76.2% to 84.5%; correspondingly, the temperature of the cooling water at the outlet of the evaporative cooler decreases from 19.8 ^{o}C to 19.3 ^{o}C, and the temperature of the cooling water at the inlet of the evaporative cooler decreases from 22 ^{o}C to 20.4 ^{o}C. Fig. 12(b) shows how varying $m_{w,EC}$ affects the humidity ratio difference of the air between the outlet and inlet of the evaporative cooler ($\Delta\omega_a$) and the moisture removal rate in the evaporative cooler (m_{EC}). When $m_{w,EC}$ increases from 0.16 kg/s to 0.27 kg/s, $\Delta\omega_a$ increases from 1.63 g/kg to 1.73 g/kg; when $m_{w,EC}$ is higher than 0.27 kg/s, $\Delta\omega_a$ remains stable. With the increase of $m_{w,EC}$, m_{EC} initially increases and then remains constant.

Fig. 13 shows how varying the mass flow rate of the spraying water, in the evaporative cooler, ($m_{w,EC}$) affects the system performance. As shown in Fig. 13(a), when $m_{w,EC}$ increases from 0.16 kg/s to 0.33 kg/s, T_{con} decreases from 41.4 ^{o}C to 40.3 ^{o}C. This is because the moisture removal rate in the evaporative cooler (m_{EC}) increases with the increasing $m_{w,EC}$, and the air temperature leaving the evaporative cooler decreases. This enhances the dehumidification effect and decreases both the solution temperature and the solution concentration at the outlet of the dehumidifier (point 11). The regeneration effect is enhanced due to the decrease of solution concentration entering the regenerator, which results

in a decreased solution temperature at the outlet of the regenerator (point 15). The temperature of the mixed solution (point 13) at the inlet of the condenser decreases, which affects the condensing temperature. In addition, $m_{w,EC}$ does not have much effects on ΔT_{sub}. Fig. 13(b) shows how the COP_{ch} and COP_{sub} are affected by varying $m_{w,EC}$. With the increase of $m_{w,EC}$, COP_{ch} increases from 3.4 to 3.55, which is mainly affected by the decrease of the condensing temperature, while COP_{sub} decreases slightly from 0.13 to 0.11 and then increases slightly to 0.12.

Fig. 13(c) shows the effect of varying the mass flow rate of the spraying water ($m_{w,EC}$) on the exergy efficiency of the chiller cycle (η_{ch}) and the integrated subcooling cycle (η_{sub}). When $m_{w,EC}$ increases from 0.16 to 0.33 kg/s, η_{ch} decreases slightly from 0.258 to 0.252 and then increases to 0.261, which is a joint result of the exergy changes of the condensing heat and power consumption of the compressor; meanwhile, η_{sub} increases significantly from 0.268 to 0.28 and then decreases to 0.266, which mainly results from the exergy changes of the condensing heat. It should be noted that η_{sub} is pretty high, even higher than η_{ch}, which indicates that the integrated subcooling cycle is an efficient way to make use of the condensing heat. In addition, the proposed system has a better performance than the traditional water-cooled chiller. As shown in Fig. 13(d), the maximum performance improvement (COP_{imp}) is 8% and the exergy efficiency improvement (η_{imp}) varies from 23.5% to 27.9%.

3.6 Economic evaluation of the use of the integrated subcooling cycle

From the above experimental results, the proposed system, with the use of the integrated subcooling cycle, could achieve a performance improvement of 18.6% under optimized working parameters. Therefore, it is of interest to evaluate the economic benefits of the integrated subcooling cycle. The proposed system is considered to supply cold energy for cooling or freezing applications all

the day, such as data centers and supermarkets, and will run 300 days/year, considering two months of maintenance and noneffective working each year. The performance improvement is assumed to be 15% considering the effect of ambient air parameters. The proposed system has a cooling capacity of 8 kW, with a project life time of 15 years. The component costs of the integrated subcooling cycle are shown in Table 4. For a complete financial analysis, some additional costs, such as mechanical costs, electrical costs, site works and commissioning costs, are considered to be 25% of the initial capital cost [24]. The residual value of the components is assumed to be 4% of the original capital cost. In China, the daily average commercial electricity rate is \$0.169/kWh, \$0.137/kWh and \$0.129/kWh in Beijing, Shanghai and Nanjing, respectively [25].

Table 5 shows the results of the economic analysis, where the inflation rate and discount rate are set to 2% and 5%, respectively. The payback period varies from 2.4 to 3.2 years based on different electricity tariffs in different cities; correspondingly, the savings to investment ratio is between 1.41 and 1.84, which indicates that the project is profitable. Effects of inflation rates and discount rates on the economic benefits of the integrated subcooling cycle are also considered for Beijing, as shown in Fig. 14. Higher inflation rates or discount rates significantly decrease the savings to investment ratio (SIR); with a given inflation rate of 4%, SIR decreases significantly from 1.81 to 1.48 as the discount rate increases gradually from 3% to 11%.

4. Conclusions

In this paper, an experimental setup of a hybrid vapor compression refrigeration system is built and tested for the first time to prove a novel refrigerant subcooling method. In this method, the heat from the condenser is used to drive liquid desiccant dehumidification for dry air which is then to absorb moisture from spray water, by which low temperature cooling water could be obtained to subcool the

refrigerant leaving the condenser. The proposed system includes a chiller cycle and an integrated subcooling cycle. Varying several key parameters affects the proposed system; these parameters include the mass flow rates of the dehumidification air (G_a), ambient air (G_{amb}), dehumidification solution ($m_{s,deh}$), regeneration solution ($m_{s,reg}$), and the spraying water ($m_{w,EC}$). Comparisons are made between the proposed system and the traditional water-cooled chiller. The main conclusions are as follows:

(1) The proposed system can achieve a larger degree of subcooling, namely 15-20 ^{o}C, using the low-grade condensing heat (around 40 ^{o}C). What's more, it has much higher performances than the traditional water-cooled chiller, with the maximum chiller performance improvement (COP_{imp}) of 18.6% and the maximum exergy efficiency improvement (η_{imp}) of 27.9%.

(2) The integrated subcooling cycle has a low COP_{sub}, around 0.1, which is due to the low-grade condensing heat. However, it has a pretty high exergy efficiency, with the maximum value of 0.28, which indicates that the integrated subcooling cycle is an efficient way to make use of the low-grade heat.

(3) The flow rate of the dehumidification air (G_a) has a large effect on the system performance. With the increase of G_a, both the COP_{ch} and COP_{sub} increase initially and subsequently decrease. The optimum G_a is around 0.25 kg/s under studied working conditions. Varying the mass flow rate of ambient air (G_{amb}) significantly affects the system performance. With the increase of G_{amb}, the COP_{ch} increases gradually, while COP_{sub} decreases generally; when G_{amb} is higher than 0.21 kg/s, both COP_{ch} and COP_{sub} change slightly.

(4) The system performance is sensitive to the mass flow rates of the dehumidification solution ($m_{s,deh}$), regeneration solution ($m_{s,reg}$) and spraying water ($m_{w,EC}$). With the increase of $m_{s,deh}$,

COP_{ch} increases gradually from 3.44 to 3.59, while COP_{sub} decreases slightly at first, and then increases slightly. When $m_{s,reg}$ increases from 0.4 kg/s to 0.66 kg/s, COP_{ch} increases from 2.9 to 3.1, while COP_{sub} decreases slightly from 0.11 to 0.1; when $m_{s,reg}$ is higher than 0.66 kg/s, both COP_{ch} and COP_{sub} do not significantly vary. With the increase of $m_{w,EC}$, COP_{ch} increases from 3.4 to 3.55, while COP_{sub} decreases slightly from 0.13 to 0.11 and then increases slightly to 0.12. In general, a higher $m_{w,EC}$ is better for the system performance.

(5) Economic analysis of the integrated subcooling cycle, with a project life-span of 15 years, shows that the payback period varies from 2.4 to 3.2 years based on different electricity tariffs in different cities in China; correspondingly, the savings to investment ratio is between 1.41 and 1.84, which indicates that the project is profitable. Both inflation rates and discount rates have a large effect on the economic benefits; the savings to investment ratio (SIR) varies significantly from 1.3 to 2.1 under studied conditions.

Acknowledgements

This work was supported by the International Collaborative Key Project of the Natural Science Foundation of China (No. 51520105009), the Research Grants Council of the Hong Kong SAR, China (UGC/FDS25/E04/17; UGC/FDS25/E10/16), and the National Science and Technology Support Project (2014BAJ01B06).

References

[1] NBS. China Statistical Yearbook. 2014, Beijing, China: National Bureau of Statistics.

[2] Pottker G, Hrnjak P. Effect of the condenser subcooling on the performance of vapor compression systems. International Journal of Refrigeration 2015;50:156-164.

[3] Klein SA, Reindl DT, Brownell K. Refrigeration system performance using liquid-suction heat

exchangers. International Journal of Refrigeration 2000;23(8):588-596.

[4] Llopis R, Sanz-Kock C, Cabello R, et al. Experimental evaluation of an internal heat exchanger in a CO_2 subcritical refrigeration cycle with gas-cooler. Applied Thermal Engineering 2015;80:31-41.

[5] Hermes CJL. Refrigerant charge reduction in vapor compression refrigeration cycles via liquid-to-suction heat exchange. International Journal of Refrigeration 2015;52:93-99.

[6] Navarro-EsbríJ, MolésF, Barragán-CerveraÁ. Experimental analysis of the internal heat exchanger influence on a vapour compression system performance working with R1234yf as a drop-in replacement for R134a. Applied Thermal Engineering 2013;59:153-161.

[7] Mota-Babiloni A, Navarro-Esbrí J, Barragán-CerveraÁ, et al. Drop-in analysis of an internal heat exchanger in a vapour compression system using R1234ze(E) and R450A as alternatives for R134a. Energy 2015;90:1636-1644.

[8] Yang L, Zhang CL. On subcooler design for integrated two-temperature supermarket refrigeration system. Energy and Buildings 2011;43(1):224-231.

[9] Qureshi BA, Zubair SM. The impact of fouling on performance of a vapor compression refrigeration system with integrated mechanical sub-cooling system. Applied Energy 2012;92(2):750-762.

[10] Llopis R, Nebot-Andrés L, Cabello R, et al. Experimental evaluation of a CO_2 transcritical refrigeration plant with dedicated mechanical subcooling. International Journal of Refrigeration 2016;69:361-368.

[11] Qureshi BA, Inam M, Antar MA, et al. Experimental energetic analysis of a vapor compression refrigeration system with dedicated mechanical sub-cooling. Applied Energy 2013;102(2):1035-1041.

[12] Llopis R, Cabello R, Sánchez D, et al. Energy improvements of CO_2 transcritical refrigeration cycles using dedicated mechanical subcooling. International Journal of Refrigeration 2015;55:129-141.

[13] Liu X, Fang GY, Chen Z. Dynamic charging characteristics modeling of heat storage device with heat pipe. Applied Thermal Engineering 2011;31:2902-2908.

[14] Hsiao MJ, Kuo YF, Shen CC, Cheng CH, Chen SL. Performance enhancement of a heat pump system with ice storage subcooler. International Journal of Refrigeration 2010;33:251-258.

[15] Huang MC, Chen BR, Hsiao MJ, Chen SL. Application of thermal battery in the ice storage air-conditioning system as a subcooler. International Journal of Refrigeration 2007;30:245-253.

[16] Hsiao MJ, Cheng CH, Huang MC, Chen SL. Performance enhancement of a subcooled cold storage air conditioning system. Energy Conversion and Management 2009;50:2992-2998.

[17] She XH, Yin YG, Dong YM, Zhang XS. Investigation on air flow patterns of evaporative cooling and dehumidification process in a hybrid refrigeration system, Applied Thermal Engineering 2016;95:79-94.

[18] She XH, Yin YG, Zhang XS. Suggested solution concentration for an energy-efficient refrigeration system combined with condensation heat-driven liquid desiccant cycle, Renewable energy 2015;83;553-564.

[19] She XH, Yin YG, Zhang XS. Analytical study on condensation heat distribution modes in a hybrid vapor compression refrigeration system, Energy and Buildings 2015;88:288-302.

[20] She XH, Yin YG, Zhang XS. Thermodynamic analysis of a novel energy-efficient refrigeration system subcooled by liquid desiccant dehumidification and evaporation. Energy Conversion and Management 2014;78:286-296.

[21] Conde MR. Properties of aqueous solutions of lithium and calcium chlorides: formulations for use in air conditioning equipment design. International Journal of Thermal Sciences 2004;43:367-382.

[22] ASHRAE, 2008a. Chapter 38-Condensers, water-cooled condensers, Heat Removal, pp. 1-8.

[23] Feibel BJ. Investment Performance Measurement, Wiley Interscience, New York, 2003.

[24] Salehin S, Ferdaous MT, Chowdhury RM, et al. Assessment of renewable energy systems combining techno-economic optimization with energy scenario analysis. Energy 2016;112:729-741.

[25] State Grid Corporation of China, http://www.sgcc.com.cn/

Figure Captions

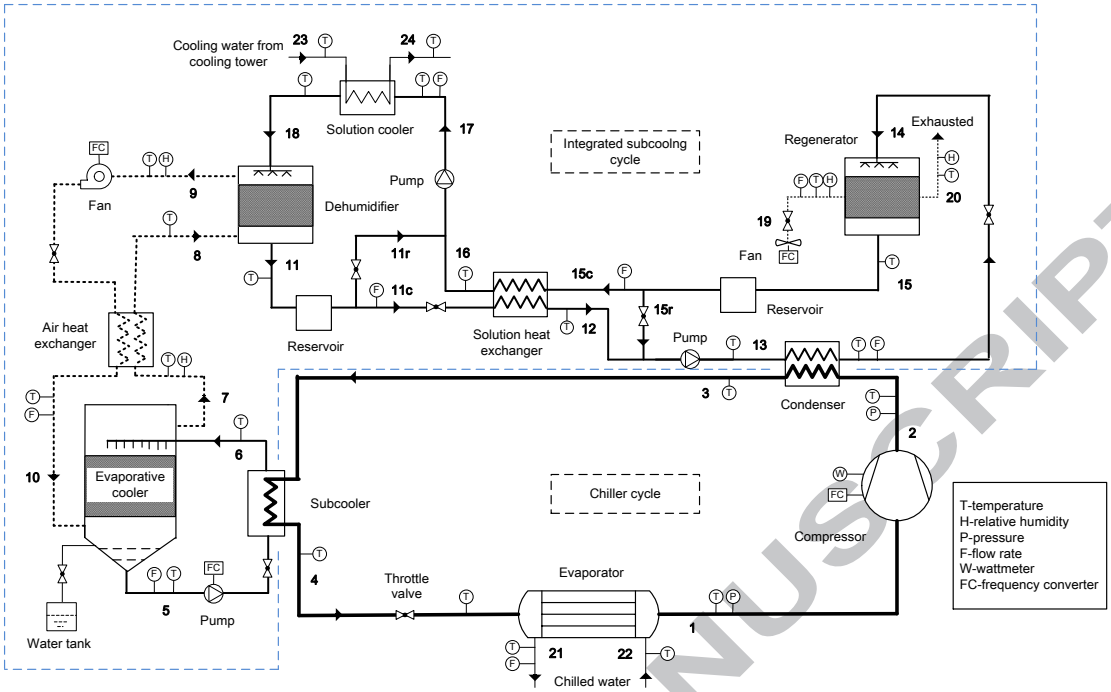

Fig. 1. Schematic diagram of the hybrid vapor-compression refrigeration system.

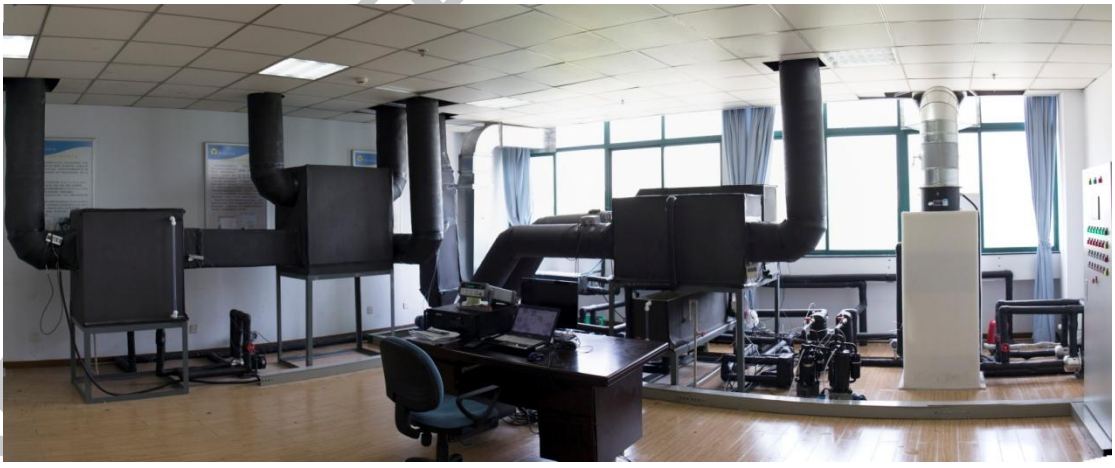

Fig. 2. Experimental setup of the hybrid vapor-compression refrigeration system.

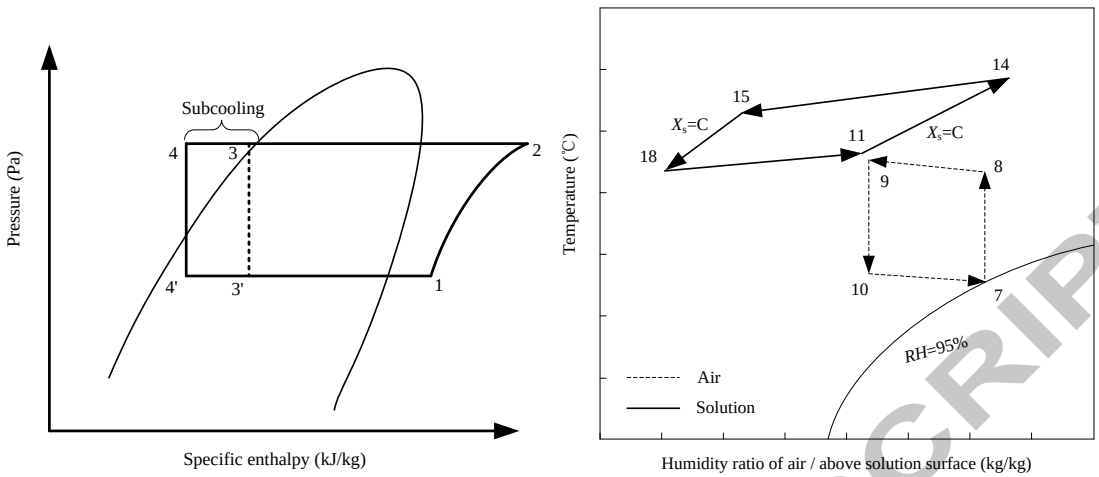

(a) (b)

Fig. 3. P-h diagram of refrigerants (a) and T-d diagram of air and solution (b).

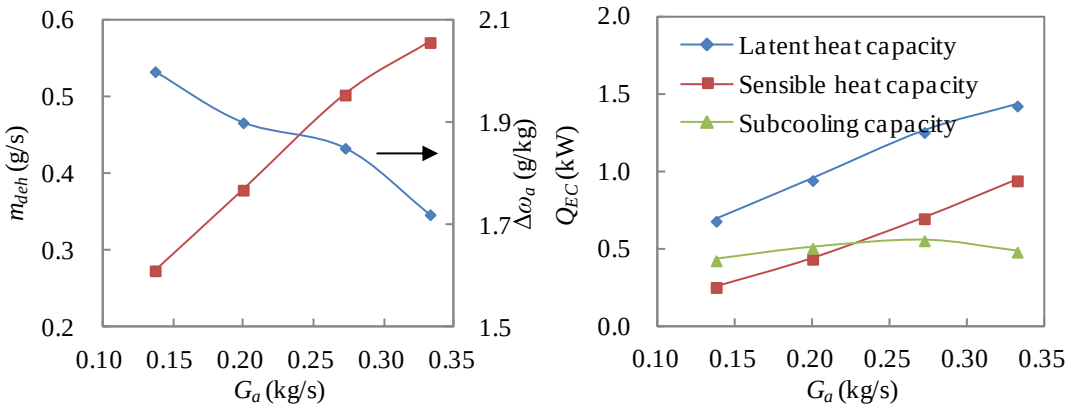

(a) (b)

Fig. 4. Dehumidifier response (a) and evaporative cooler response (b) due to varying the mass flow rate of dehumidification air.

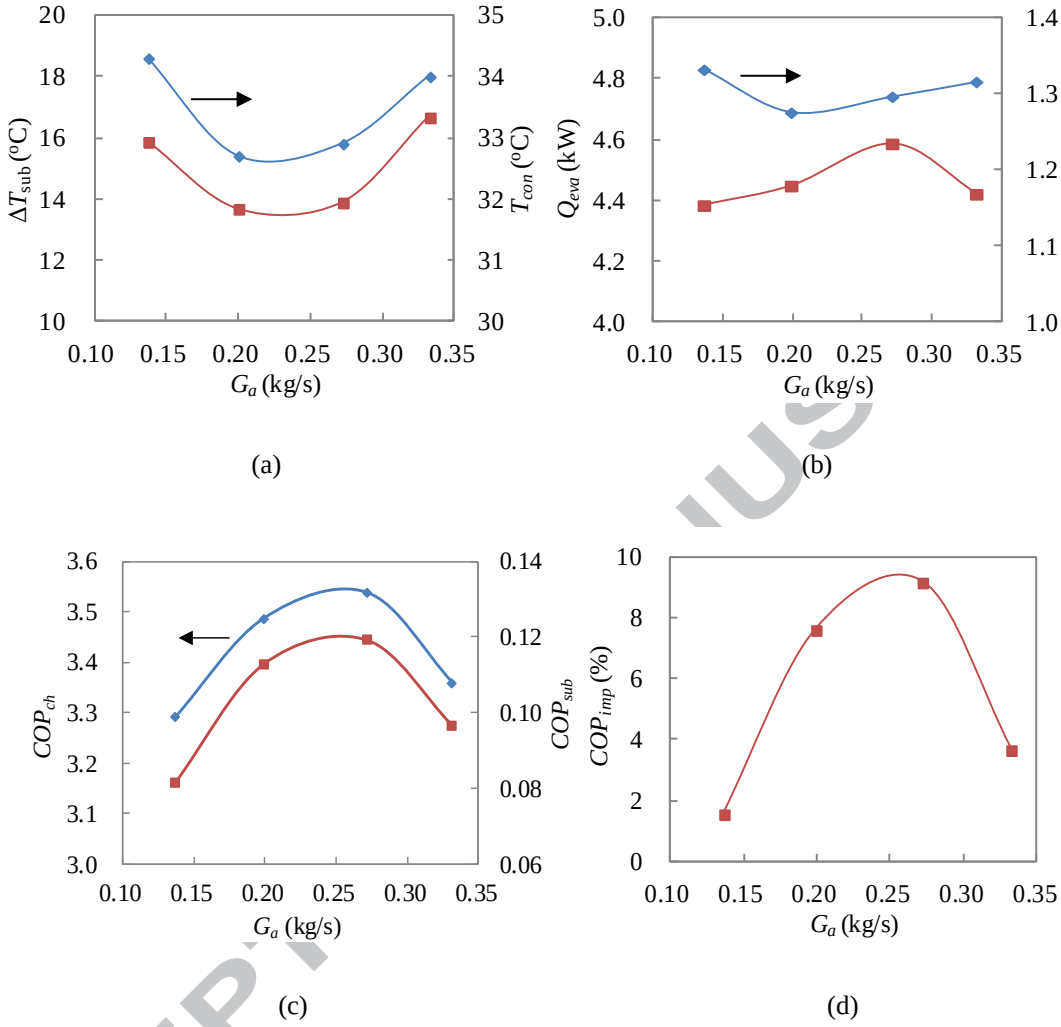

Fig. 5. Change in system performance due to varying the mass flow rate of dehumidification air.

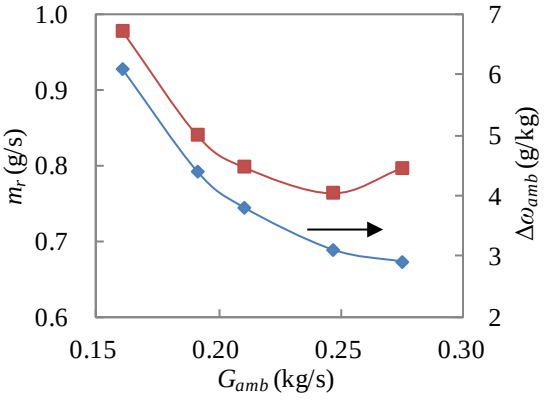

Fig. 6. Regenerator response due to varying the mass flow rate of ambient air.

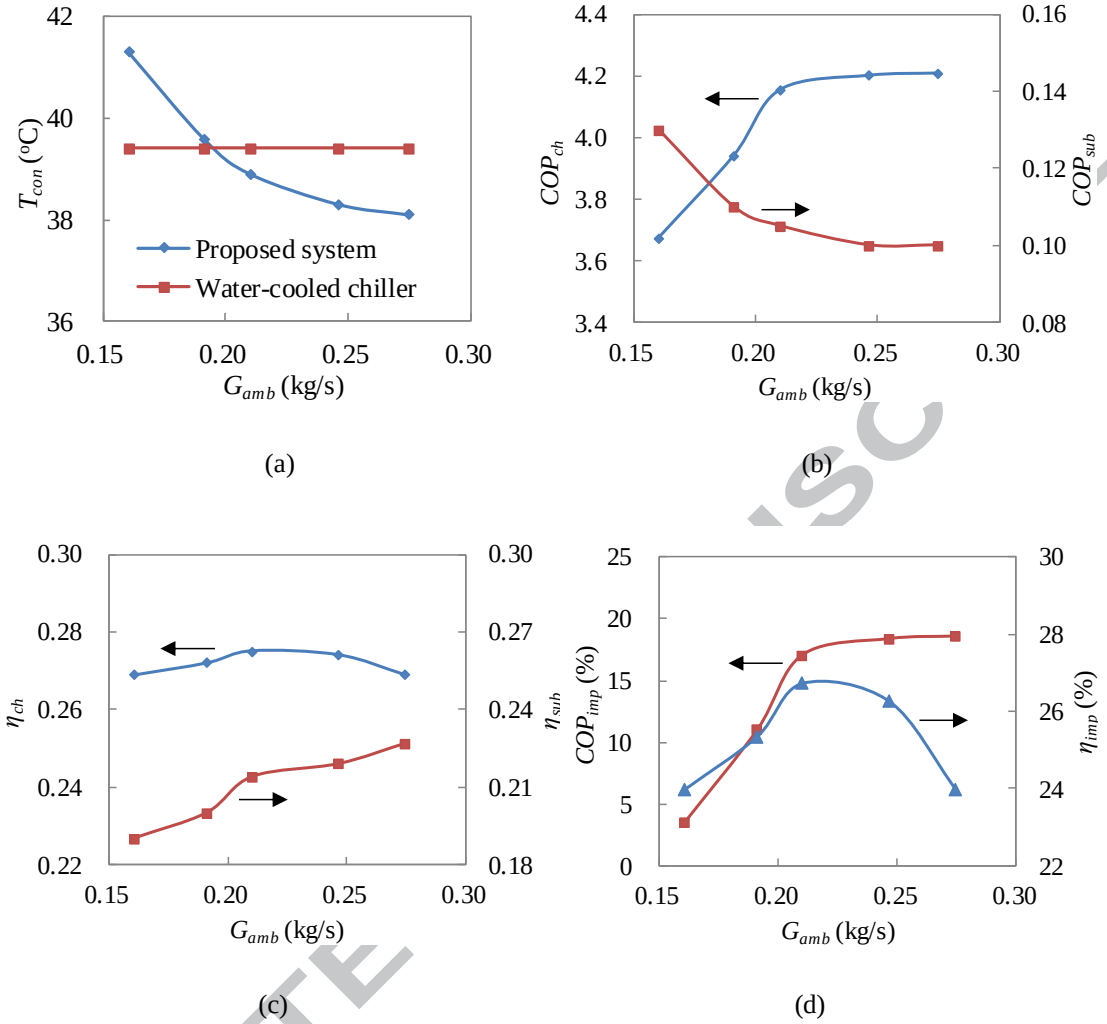

Fig. 7. Change in system performance due to varying the mass flow rate of ambient air.

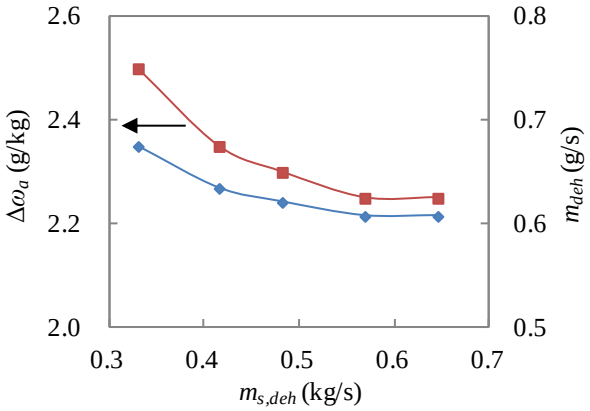

Fig. 8. Change in the dehumidifier performance due to varying the mass flow rate of dehumidification solution.

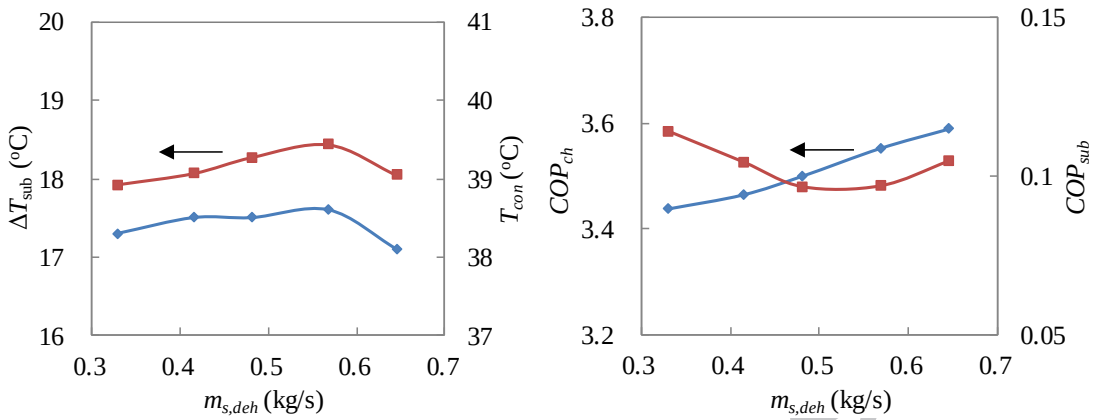

(a) (b)

Fig. 9. Change in system performance due to varying the mass flow rate of dehumidification solution.

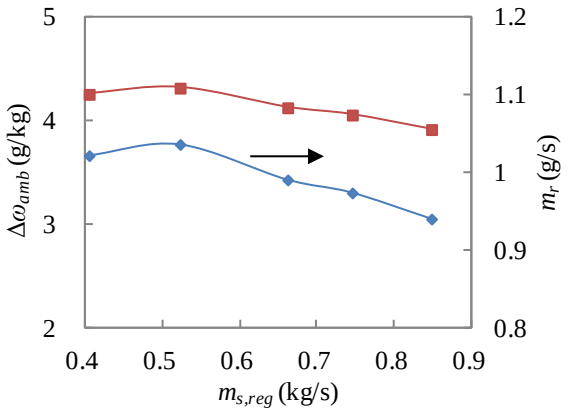

Fig. 10. Regenerator response due to varying the mass flow rate of regeneration solution.

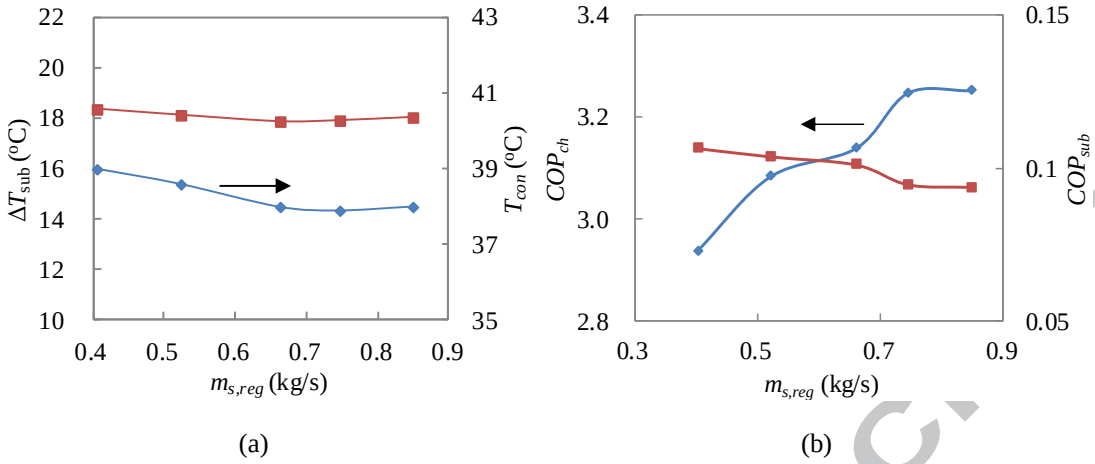

Fig. 11. Change in system performance due to varying the mass flow rate of regeneration solution.

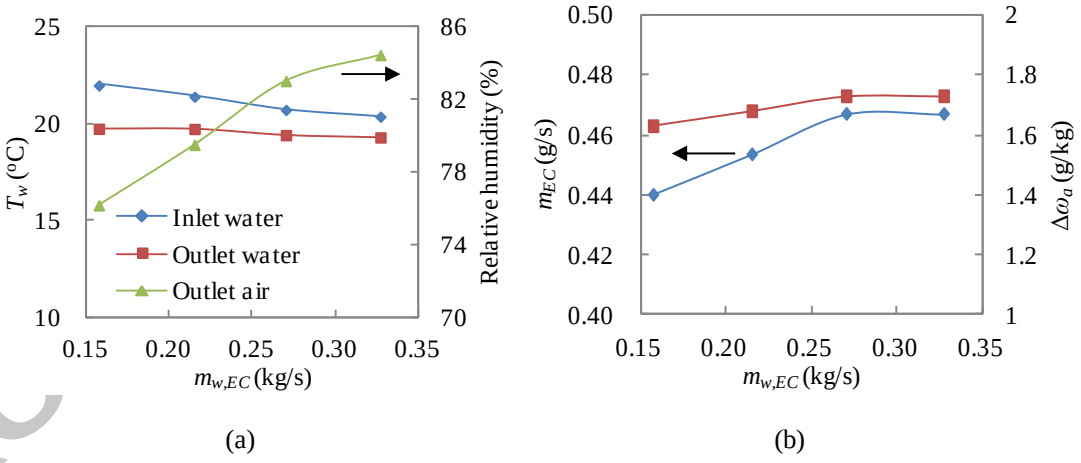

Fig. 12. Change in evaporative cooler performance due to varying the mass flow rates of spraying water.

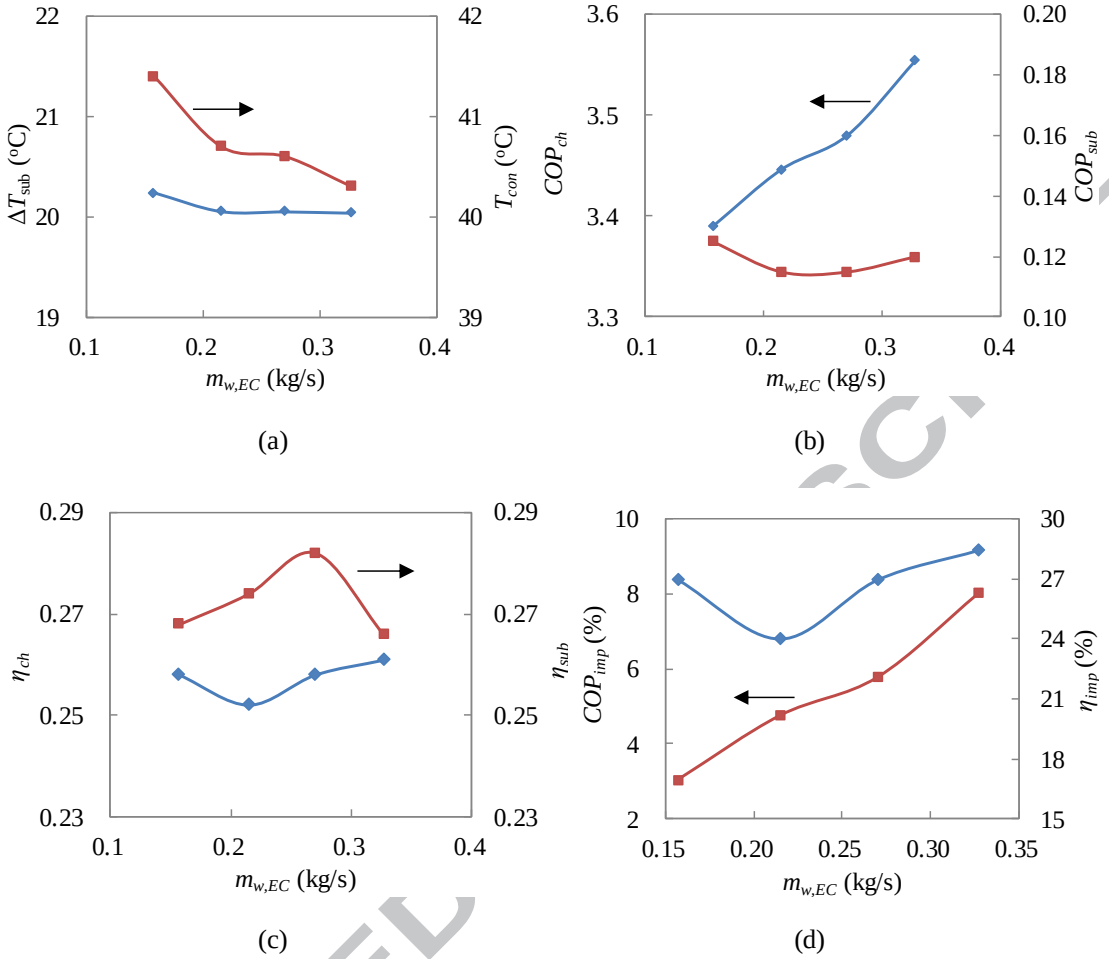

Fig. 13. Change in system performance due to varying the mass flow rate of spraying water.

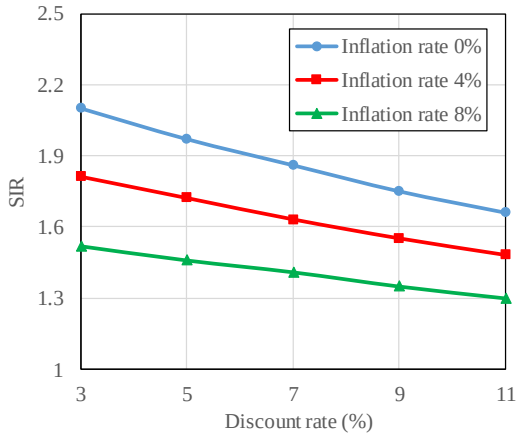

Fig. 14. Effects of inflation rates and discount rates on the economic benefits of the integrated subcooling cycle.

Table 1 Parameters of measuring instruments.

Devices	Parameters	Range	Uncertainty
Turbine flowmeter	Water flow rate	0.6-6.0 m^3/h	±0.38%RD
		0.2-1.2 m^3/h	±0.56%RD
KIMO flow meter	Air flow rate	0-99999 m^3/h	±1.5%RD
Electromagnetic flow meter	Solution flow rate	0.16-2.5 m^3/h	±0.5%FS
		0.4-6.0 m^3/h	±0.5%FS
WT230 power meter	Power consumption	Auto	±0.1%RD
Rotronic temperature and	Air temperature and	-40-60 ^oC	±0.1 ^oC
humidity transmitter	humidity	0-100% RH	±0.8% RH
Thermocouple (T-type)	Water/solution temperature	-10-120 ^oC	±0.1 ^oC
Pt100 platinum resistor	Refrigerant temperature	-200-350 ^oC	±0.15 ^oC
Pressure transmitter	Refrigerant pressure	0-2.5 MPa	±0.1%RD

Table 2 Energy balance of the chiller cycle.

$m_{w,eva}$ (kg/s)	T_{22} (^oC)	T_{21} (^oC)	W_{com} (kW)	$m_{s,reg}$ (kg/s)	T_{13} (^oC)	T_{14} (^oC)	$m_{w,EC}$ (kg/s)	T_5 (^oC)	T_6 (^oC)	Q_{in} (kW)	Q_{out} (kW)	E (%)
0.42	15.6	12.2	1.4	0.56	31.7	34.8	0.27	20.6	22.2	7.4	7.1	4.1
0.42	15.7	12.3	1.4	0.56	32.3	35.4	0.27	21.1	22.6	7.4	7.0	5.4
0.42	15.7	12.5	1.5	0.56	34.4	37.9	0.27	20.5	21.4	7.1	7.1	0
0.42	15.9	12.6	1.4	0.56	33.3	36.4	0.27	21.6	23.2	7.1	7.2	1.4
0.42	16.0	12.5	1.4	0.56	32.7	35.9	0.27	21.4	23.0	7.4	7.4	0
0.43	16.0	13.0	1.5	0.58	34.8	38.1	0.22	19.8	21.4	6.8	7.4	8.1
0.43	9.9	7.5	1.3	0.58	27.2	30.1	0.27	16.6	17.7	5.7	6.3	9.5
0.45	12.6	9.6	1.4	0.58	32.0	34.5	0.27	19.0	21.1	6.8	6.9	1.4
0.45	13.0	10.2	1.4	0.58	32.3	35.0	0.27	19.1	21.2	6.7	7.1	5.6
0.45	13.0	10.2	1.4	0.58	32.3	35.0	0.27	19.1	21.1	6.8	7.1	4.2

Table 3 Working parameters of the hybrid vapor-compression refrigeration system.

G_a (kg/s)	G_{amb} (kg/s)	$m_{s,deh}$ (kg/s)	$m_{s,reg}$ (kg/s)	$m_{w,EC}$ (kg/s)	X_s (%)	$m_{w,eva}$ (kg/s)	T_{amb} (^oC)	ω_{amb} (g/kg)
0.14-0.33	0.25	0.57	0.57	0.27	27.3	0.42	29.5-30.6	7-7.5
0.27	0.16-0.27	0.56	0.56	0.27	25.6	0.42	31.6-32	13-13.3
0.27	0.24	0.33-0.65	0.58	0.27	27.5	0.45	31.5-32	9-9.3
0.27	0.24	0.57	0.4-0.85	0.27	27.7	0.45	31-31.7	8.3-8.7
0.27	0.24	0.54	0.59	0.16-0.33	28.5	0.42	31.7-32.4	12.9-13.2

Table 4 Component cost summary (net present cost) of the integrated subcooling cycle in the project life time.

Component	Capital ($)	Replacement ($)	O&M ($)	Residual value ($)
Regenerator	292	232	78	-6
Dehumidifier	249	197	66	-5
Evaporative cooler	253	201	68	-5
Heat exchangers	1,293	2,086	345	-25
Fans	200	323	53	-4
Pumps	563	908	150	-11
Additional cost	713	-	-	-

Note: Capital and replacement costs are from the manufacturers.

Table 5 Financial analysis results of the integrated subcooling cycle.

Performance indexes	Cities in China		
	Beijing	Shanghai	Nanjing
Total present value of investment ($)	8,215	8,215	8,215
Total present value of savings ($)	15,156	12,286	11,569
Net present value ($)	6,941	4,071	3,354
Savings to investment ratio	1.84	1.5	1.41
Simple payback period (years)	2.4	3.0	3.2

Highlights

- A novel refrigerant subcooling method is experimentally studied for the first time.
- Condensation heat is used to drive an integrated cycle to subcool the refrigerant.
- *COP* and exergy efficiency are improved by 18.6% and 27.9% respectively.
- Effects of key parameters on the system performance are disclosed.
- Economic analysis shows payback period varies from 2.4 to 3.2 years.